(Preprint) AAS 09-137

A CUBED SPHERE GRAVITY MODEL FOR FAST ORBIT PROPAGATION

Brandon A. Jones, George H. Born, and Gregory Beylkin[y]

The cubed sphere model of the gravity field maps the primary body to the surface of a segmented cube, with a basis defined on the cube surface for interpolation purposes. As a result, the model decreases orbit propagation time and provides a localized gravity model. This paper provides a brief description of the cubed sphere model, which is currently derived from the spherical harmonics. Early tests of the integration constant did not meet requirements, thus the model was reconfigured to improve accuracy. A detailed characterization of the model was then performed

A new model, the cubed sphere, was developed to localize the gravity field and decrease the model evaluation time.[1] At its core, the cubed sphere is an interpolation model that relies on a localized basis defined on the surface of a segmented cube. This cube is mapped to a sphere to represent spherical objects. This paper explores applications of this cubed sphere model to orbit propagation, particularly how it compares to the spherical harmonics model solutions.

THE CUBED SPHERE MODEL

Originally proposed by Beylkin and Cramer,[1] the cubed sphere model definespheaBeyla8nallymoethod2n96(mo)]TJ
rncclalrition gHenc, spherers by mape6(ap4sb-a(by)-26nal(n

The geopotential values computed by the remaining base model are then used to define the basis functions on the surface of the cube. Although other formulations are possible, B-splines are currently used. The method for deriving the cubed sphere will now be defined.

A major property of the cubed sphere model that must be defined is the grid size, N. Similar to the degree and order of the spherical harmonic model, the grid size is a measure of model fidelity and defines the density of the grid on each cube panel. For a given altitude, the values of latitude and longitude are segmented such that

$$= 2 \quad x; \qquad = 2 \quad y \tag{2}$$

where x and y are discrete values in the range $[0; 1)$ with spacing N^{-1}. It may not be readily apparent why the latitude, , is in the range $[0; 2 \ )$, but this will be understood in a moment.

Latitude and longitude have been mapped to a two dimensional grid specified by x and y to solve for the B-spline interpolation scheme. As described in the appendix, the interpolation coefficients are easily derived in the Fourier domain for a periodic, two dimensional plane. If the grid variables x and y are 1-periodic, then the two-dimensional FFT algorithm may be used. The values of potential at grid intersection points are used as data values. Hence, given a cube is comprised of six planes, the FFT algorithm provides a simplified method for representing the potential on the surface of a cube.

If only varies from =2 to =2, or 0 to , then y is not 1-periodic. Thus, the formulation of the Earth's geopotential must be duplicated to complete the period. The mathematical formulation of the new geopotential, U_p, is then

$$U_p(r; \ ; \ ) = \begin{cases} U(r; \ ; \ ) & \text{if } 0 \quad < \ ; \\ U(r; 2 \quad ; \ + \ ) & \text{if } \quad < 2 \end{cases} \tag{3}$$

and is now a value in the range $[0; 2 \ )$ and 2 -periodic. Thus, y is now 1-periodic and the FFT algorithm is used to generate the B-spline interpolation coefficients. Note the doubling of the geopotential model is only used to generate these coefficients.

To prevent grid distortion given the ambiguity of longitude at the poles, the Earth is rotated so that the poles lie along the equator. This is equivalent to the transverse mercator map projection. A second x-y plane is generated after this rotation, with the FFT algorithm applied and a second set of B-spline coefficients determined. This rotation is performed in the formulation of the base model.

B-spline coefficients have been defined over the flat surface of the two x-y grids. The grids are then broken into appropriate segments to generate the faces of a cube. Each face, or panel, of the cube has a new x-y grid with axes defined over the range $[-1; 1]$. Four panels along the middle latitudes are selected from the first plane, while the two remaining panels along the poles are selected from the second plane. Grid spacing is preserved along the face of the cube, however the new panels are a quarter of the size. Thus, the size of the grid on each panel is $N/4$ by $N/4$. This property is used in the naming convention defined for a given model. A CS-X model is a cubed sphere model where X corresponds to the grid size on a cube face , or N=4. Finally, the geopotential model for the given shell has now been defined and is represented as a cube.

Additionally, a user specified number of nested, concentric shells is defined for interpolation in the radial direction. Shell spacing is determined by defining a set number of points (h_j) equally

spaced in the interval $[0; 1]$. Shell locations are then

$$\frac{R}{r_j} = 1 \quad h_j^2 \tag{4}$$

where r_j is the radial distance of the shell. These ratios, which represent a distance above the planet's surface in the range $(0; 1]$, define shell locations. As the ratio approaches zero, the orbit radius approaches infinity. Shell density increases as altitude decreases, corresponding to the inverse square relationship between geopotential and radius. The final shell at a radius of infinity is not computed. The model assumes eventual decay to zero of the spherical harmonic terms, thus the two-body equation will govern satellite dynamics.

These primary shells are modeled with each consisting of subshells for polynomial interpolation of a prescribed degree in the radial direction. For a fifth degree interpolation scheme, six subshells are required. The spacing between subshells is mapped to the range $[\quad 1; 1]$ where zero corresponds to the midpoint between primary shells. The subshells are then located at the Chebyshev nodes based on the degree of the polynomial. Chebyshev nodes were selected to minimize interpolation error due to node selection. Each primary and subshell is independent of all others, thus there is no coupling in model generation. B-spline coefficients for each shell are generated as previously described using the applicable altitude for the evaluation of Eq. 3. A total of $(l + 1) \quad M$ shells are computed where l is the degree of the interpolating polynomial and M is the number of primary shells. It is important to note the mapping notesilyis foand

describbeinh2442spepeci5(fl(ayor)-442(cooncients24426(of)]TJ 0 -13.549 Td acc(seneratime,)8259(are)8322t(will)8178(rep

Model Configuration

Test software was written to evaluate the model at a user defined number of random points above the primary body. For each point, the cubed sphere model is compared to the base model and the L_1 norm is evaluated. The maximum norm of all points is then used to characterize the accuracy of the model. Tests utilized 10^5 random points, with any increases yielding similar results. The original cubed sphere model differed from the spherical harmonics by as much as 10 m/sec^2. Although this value may appear rather small, the model was reconfigured and accuracy was improved to 10^{-11} m/sec^2, and 10^{-14} m/sec^2 for lower fidelity models. The main focus of this reconfiguration was to improve model performance for higher fidelity models, i.e. equivalents to the 70x70 models and those of higher degree and order. Full benefits of the reconfiguration will be demonstrated in the section discussing the integration constant performance.

Table 2. Cubed Sphere Configuration

Property		Before	Current
Number of parameters estimated (P)		3	4
B-spline degree (m)		11	11
Chebyshev polynomial degree (l)		5	11
Number of primary shells (M)		13	13
Grid Density (N) for:	CS-30 / 20x20	80	120
	CS-76 / 70x70	280	304
	CS-162 / 150x150	600	648

Changes to the cubed sphere configuration made in the course of this research, along with other major properties, are included in Table 2. Note the change in Chebyshev polynomial degree and grid density did result in a file size increase. Additionally, the original model did not include the estimate of the potential at a given point. Of course, these configuration parameters can be tailored to a specific design based on orbit accuracy requirements and file size limitations. If the potential is not required, the file size is reduced by almost 25%. Table 2 defines the base models for the CS-30, CS-76, and CS-162 models used throughout this study. Other changes were made to the software to improve computation speed and switch from the unnormalized to normalized formulation of the associated Legendre functions in the base model. Finally, the model storage scheme of the B-spline coefficients was altered to allow for loading of selected shells to reduce software memory requirements and decrease initialization time.

The number of elements that must be stored in the model are computed using

$$\textit{Number of elements} = 6P(l+1)M\left(\frac{N}{4}+m\right)^2 \tag{5}$$

where the meaning of the terms are found in Table 2 or the notation section. Additionally, there is some memory overhead associated with the file header. For the CS-30 model, this results in a 49 Mb file. Similarly, a 856 Mb file is required for a CS-162 model. However, the complete model is not required for most applications. Since the model is localized, only the primary and secondary shells required for a given orbit must be generated or loaded into memory.

Experimental results demonstrate the evaluation time of the cubed sphere model is slightly more than the 20x20 spherical harmonics. As the model grid density is increased, corresponding to an increase in model fidelity, evaluation time does not increase. The B-spline coefficients are organized such that no search is necessary. If the degree of the interpolating functions remains constant for each grid size, model evaluation time remains constant. Thus, speed-up factors compared to the spherical harmonics increases with model fidelity.

COMPARISONS TO THE SPHERICAL HARMONICS MODEL

After the cubed sphere was fully developed, it was compared to the spherical harmonics model. The GGM02C[10] model was selected as both the base model of the cubed sphere and the basis of comparison for the following tests. Evaluations included a comparison of the integration constant, spatial comparisons of the models in the form of gravity anomaly plots, and finally the propagated orbits themselves.

The TurboProp orbit integration package[11] was used to minimize software development time. This software provides integration tools implemented in C that are compatible with MATLAB. Unreleased versions are also compatible with Python. The cubed sphere model, along with the necessary interface code, was implemented within the TurboProp framework. However, the software can be easily ported to other packages. For the following tests requiring orbit propagation, the Tur-

the geopotential and the gravity accelerations. However, this will drastically increase file size. Additionally, finite differencing would only be an approximation.

Instead of testing the cubed sphere under the Laplace criterion, another technique using the Jacobi-like integration constant,[12]

$$K = \text{[illegible]}$$

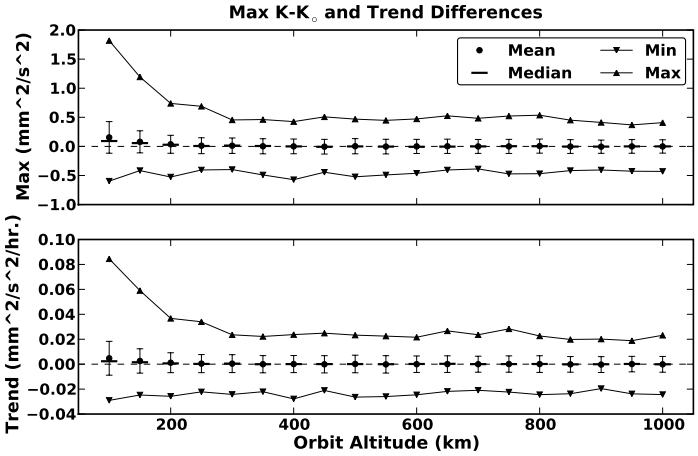

Figure 4 Comparison of the integration constant variations for the CS-70 model with the spherical harmonics base model. Error bars are 1- .

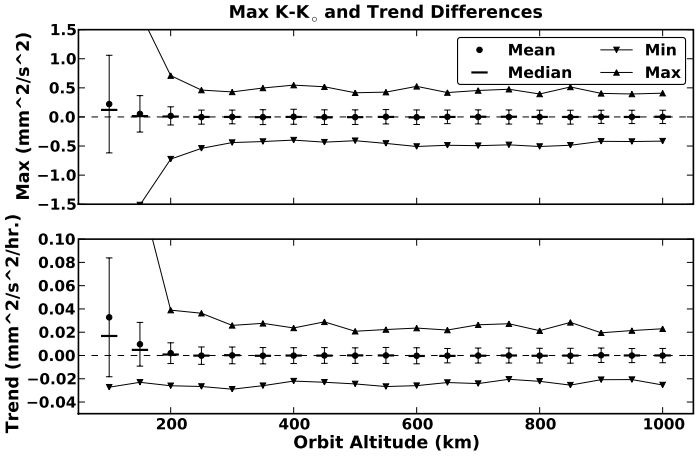

Figure 5 Comparison of the integration constant variations for the CS-150 model with the spherical harmonics base model. Error bars are 1- .

Results for the CS-162 model are provided in Figure 5. Note some extreme values have been truncated to improve visibility of performance statistics at higher altitudes. In the case of the differences in the magnitude differences, the minimum values for the 100 and 150 km orbits are -3.39 and -1.51 mm^2/sec^2, respectively. The maximum values are 5.20 and 1.79 mm^2/sec^2. In the case of the trend slope differences, the missing maximums are 0.44 and 0.14 mm^2/sec^2/hour. Like the CS-76 model, differences between the cubed sphere and spherical harmonics models are greater at lower altitudes. This trend remains consistent through the remaining tests, and is attributed to the greater differences in the gravity anomalies at lower altitudes seen in the next section. In this case, the differences in the models settles around 250 km.

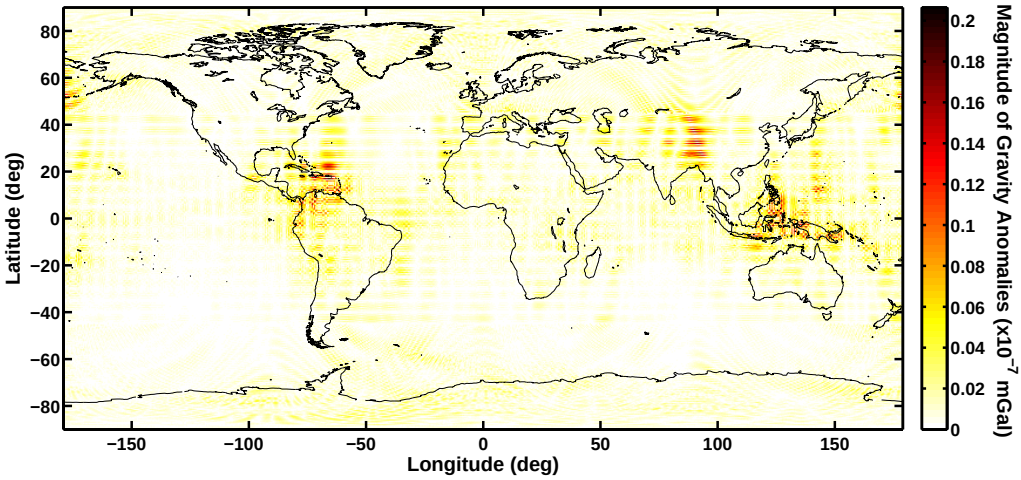

Figure 7. CS-162 gravity anomalies at 300 km

included, but yielded similar results to the previous two models. The grid spacing was visible, but the regions of higher differences were not as isolated as the CS-162 case.

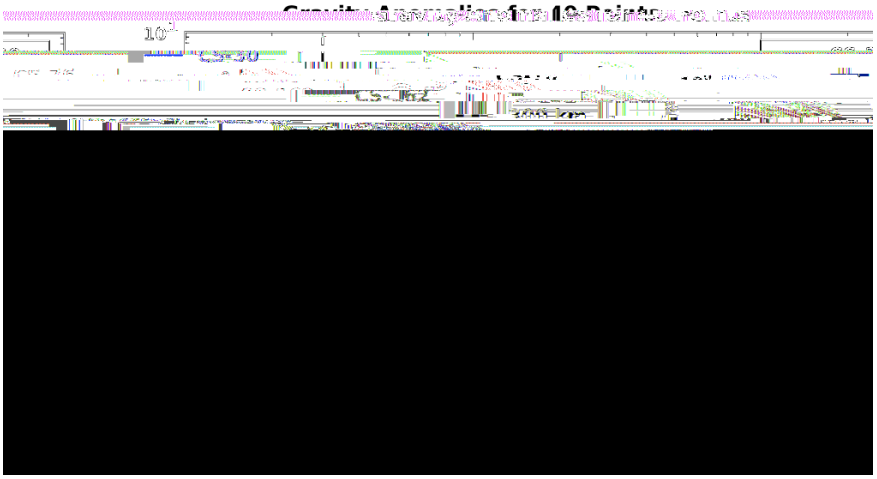

Figure 8 Variations in gravity anomalies with altitude for 42 points on the Earth using the CS-30, CS-76, and CS-162 models.

To illustrate gravity anomaly variations with altitude, Figure 8 illustrates the difference in gravity anomalies for each of the models for altitudes up to geosynchronous orbit. Most of the forty points depicted were randomly selected, although a couple of points were chosen to coincide with regions of expectedly large anomalies, such as the Himalayan mountains. As expected, peak variations in the cubed sphere model with respect to the spherical harmonics occur at lower altitudes. Additionally, the largest anomalies occur for the higher fidelity models. At various altitudes, the differences become discretized due to machine precision and the relatively low contribution the perturbations

modeled by the cubed sphere have on the overall gravity acceleration.

For the CS-162 model, there is a region below 300 km and around 10^{-10} mGal where the variations are periodic. In this case, the difference is close to the machine precision and is not determined by the grid spacing. Given the Chebyshev interpolation between shells, approximation error will vary based on proximity to the nearby shells. Thus, as the altitude increases for this point in Figure 8

execution of the RK78 algorithm, and did not include file load times or software initialization. As expected, the file load time for the cubed sphere is longer than the spherical harmonics, however

all others are within 0.015 mm of the spherical harmonics. The spatial distribution of the velocity errors roughly corresponds to the position errors, with a minimum of 2.503x10 mm/sec and a maximum of 2.037x10 ^{5} mm/sec. The median 3D RMS velocity error was 3.80x10 mm/sec.

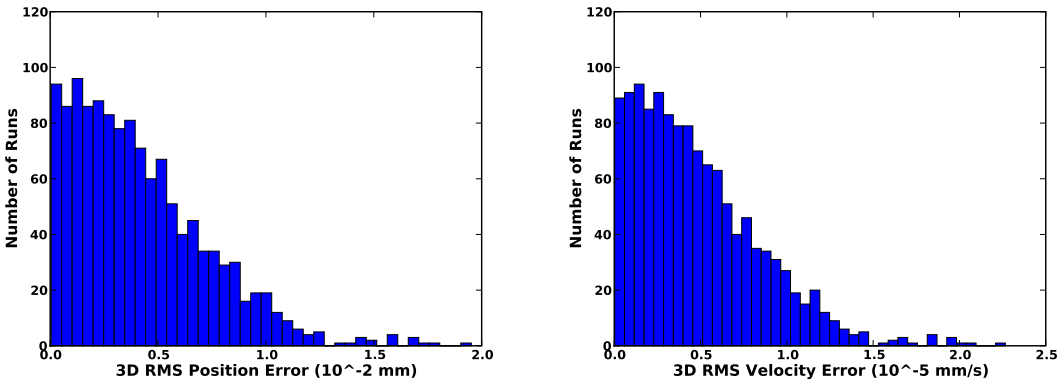

Figure 12 Distribution of 3D RMS differences for propagated orbits initially at 300 km with the CS-30 model.

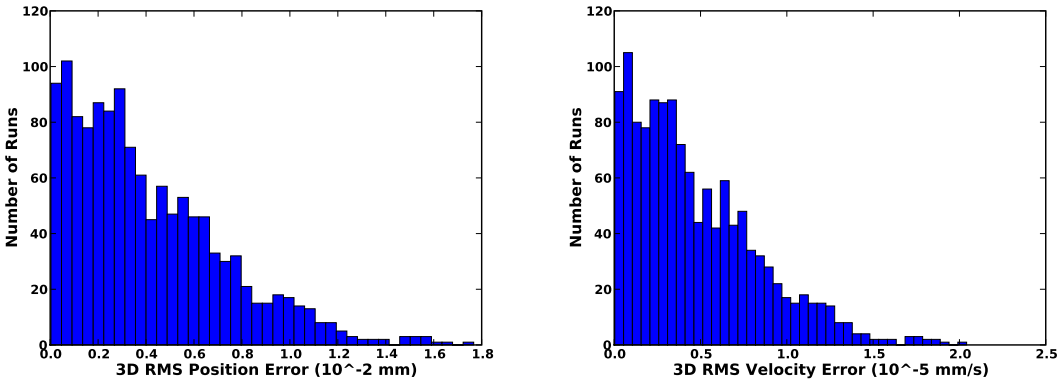

Figure 13 Distribution of 3D RMS differences for propagated orbits initially at 300 km with the CS-76 model.

Histograms of the propagation state errors for the CS-30 and CS-76 models at 300 km are provided in Figures 12 and 13, respectively. Contour plots of these errors for the CS-30 and CS-76 model have not been included since results were similar to those seen for the CS-162 model. Any accuracy differences in the results are visible in the histogram plots.

The CS-30 model position 3D RMS errors were within 0.02 mm, and as small as 4.701x10 ^{5} mm. The median value was 0.0036 mm. The velocity errors had a median of 4.11x10 mm/sec, and ranged between 2.993x10 and 2.266x10 ^{5} mm/sec. These results were roughly the same as those for the CS-162 model. Only twenty orbits had 3D RMS position errors above 0.0125 mm, and 17 had velocity errors above 1.5x10 ^{5} mm/sec.

Orbit propagation differences for the CS-76 model were roughly the same as those of the previous two models. The minimum 3D RMS error was 3.246x10 ^{5} mm, with a maximum of 0.0177 mm.

The median was 0.0033 mm. The velocity errors were less than 2.042x10 ^{5} mm/sec, with a median of 3.788x10 mm/sec. The minimum error was 2.042x10 mm/sec.

CONCLUSIONS

Results demonstrate that the cubed sphere model closely approximates the base model, in this case the spherical harmonics. Orbit propagation tests demonstrated model agreements on the order of fractions of a millimeter, and position results are summarized in Table 5. The cubed sphere model equivalent to a 150x150 spherical harmonics was over 40 times faster. However, the spherical harmonics was slightly faster for the lower fidelity model. Future research will seek to further customize the model to improve computation efficiency for these lower fidelity models.

Table 5. Cubed Sphere Position 3D RMS Performance at 300 km

Model	Min (nm)	Max (mm)	Mean (mm)	Median (mm)
CS-30	47.0	0.0200	0.0042	0.0031
CS-76	32.5	0.0177	0.0041	0.0033
CS-162	57.1	0.0176	0.0040	0.0033

The new configuration of the cubed sphere demonstrated model improvement. Fluctuations in the integration constant were greatly reduced, with less than 1% of the orbits tested exhibiting fluctuations that differed by more than an order of magnitude between the cubed sphere and the spherical harmonics model. Changes in the integration constant, including the maximum fluctuation for a given orbit and the long term trend, are consistent between the two models. For the higher fidelity models, performance is reduced below 200 km. In some cases, the cubed sphere performs better than the spherical harmonics, probably due to slight smoothing of the model when interpolating between the nodes on the surface of the cube. Gravity anomalies were also reduced, and are now within 10 mGal for all altitudes above the Earth, and less less than 10 mGal for altitudes at or above 300 km.

Future research will include integrating the cubed sphere with the orbit determination process for both Earth and Moon based missions. Even though second derivatives currently are not included in the cubed sphere, integration with nonlinear filters, such as the unscented Kalman,[13] is rather straightforward.

Unfortunately, characterizations of moon based models were not included here. Due to the relatively extreme gravity variations due to mass concentrations caused by asteroid impacts,[6] initial results demonstrated that additional tuning of the cubed sphere for lunar applications is required. Additionally, lower altitude orbits are desirable at the moon. This is a small concern considering the cubed sphere exhibited reduced performance below 300 km. However when the ratio of the primary

CA55(.CKNO)0(mWLEDGMENT)]TJ/F80 10.9091 Tf 10.909 -20.9856Td [(CA5222(loa)18(eg)-2226(prtuon)-232

AFOSR grant FA9550-07-1-0135. The authors would like to thank Keric Hill, formerly of the Colorado Center for Astrodynamics Research, who wrote the early versions of TurboProp.

NOTATION

U	geopotential
	gravitational parameter (km^3/sec^2)
$\vec{r}; r$	position vector and magnitude for the satellite (km)
	geocentric latitude (rad)
	longitude (rad)
R	equatorial radius of the primary body
n	spherical harmonics model degree
m	spherical harmonics model order
$P_{n;m}$	associated Legendre function of x with degree and order m and n
$C_{n;m}$	cosine coefficient of spherical harmonics
$S_{n;m}$	sine coefficient of spherical harmonics
N	number of lines used to segment a plane
P	number of cubed sphere parameters estimated
I	Chebyshev polynomial degree
M	number of primary shells in cubed sphere
	right ascension of the ascending node
i	inclination
K	Jacobi like integration constant
$\vec{\dot{\imath}}$	primary body rotation vector
B_m	B-spline of degree m
L_m	interpolating spline of degree m
	B-spline interpolation coefficient
$g(x)$	generic continuous function

REFERENCES

[1] G. Beylkin and R. Cramer, "Toward Multiresolution Estimation and Efficient Representation of Gravitational Fields," *Celestial Mechanics and Dynamical Astronomy*

[9]

where L_m are interpolating splines, i.e.

$$L_m(l) =$$